The Journal of Chemical Physics

RAPID COMMUNICATION | MAY 06 2025

Acidifying the Madrid-2019 force field: A rigid model for H_3O^+ with scaled charges

S. Blazquez ; M. de Lucas ; C. Vega ; F. Gámez

J. Chem. Phys. 162, 171101 (2025)
https://doi.org/10.1063/5.0267223

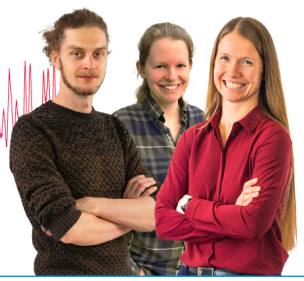

The Journal of Chemical Physics COMMUNICATION pubs.aip.org/aip/jcp

Acidifying the Madrid-2019 force field: A rigid model for H_3O^+ with scaled charges

Cite as: J. Chem. Phys. 162, 171101 (2025); doi: 10.1063/5.0267223
Submitted: 23 February 2025 • Accepted: 16 April 2025 •
Published Online: 6 May 2025

S. Blazquez, M. de Lucas,[a] C. Vega, and F. Gámez[b]

AFFILIATIONS

Depto. de Química Física I, Fac. Ciencias Químicas, Universidad Complutense de Madrid, 28040 Madrid, Spain

[a]**Current address:** IMDEA Nanoscience, Faraday 9, Campus de Cantoblanco, 28049 Madrid, Spain.
[b]**Author to whom correspondence should be addressed:** frgamez@ucm.es

ABSTRACT

A classical and rigid force field for the oxonium cation, H_3O^+, optimized in solutions of TIP4P/2005 water, is introduced. While the charges of both H_3O^+ and the selected counteranions (i.e., Cl^-, Br^-, I^-, and NO_3^-) are scaled by a factor of 0.85, following the philosophy of the so-called Madrid-2019 model for ions, the charge distribution of H_3O^+ was derived within the framework of the self-consistent atomic dipole-corrected Hirshfeld approach. Considering the simplicity of the model, the agreement between experimental data and molecular dynamics simulation results for the curvature of the solution density as a function of the solute concentration is remarkable. However, limitations persist in capturing ion-pairing behavior and long-range hydrogen-bonding dynamics in polyatomic systems. We found that a scaled charge of 0.85*e* provides an accurate description of the local structure of hydrogen halides but is detrimental to predicting the viscosity of the solution. The opposite effect is observed for HNO_3. Nonetheless, the newly optimized potential parameters for H_3O^+ expand the family of ions with scaled charges in the Madrid–2019 force field, providing a computationally efficient and versatile platform to study electrolyte solutions in acidic environments. These findings contribute to the advancement of molecular modeling techniques and to improving our understanding of the interplay between local structure (solvation, ion pairing) and transport properties in complex systems.

The oxonium ion (H_3O^+) plays a fundamental role in chemical, biological, and physical phenomena, particularly as a central species in proton transfer processes in aqueous environments. Its relevance spans the understanding of solution acidity, acid-base equilibria, and catalytic mechanisms in both organic chemistry and biological systems. The dynamics of proton transfer in water is intimately linked to the Grotthuss hopping mechanism, where the proton propagates through a coordinated series of hydrogen bond (HB) rearrangements.[1] Technologically, its high mobility is crucial in energy storage and conversion devices, such as proton conductors in fuel cells and proton exchange membranes.[2–5] Structurally, the H_3O^+ ion is surrounded by a network of HBs with neighboring water molecules, leading to tightly hydrated proton complexes of different geometries and stabilities, such as the well-known Zundel ($H_5O_2^+$) and Eigen ($H_9O_4^+$) cations, extensively studied using experimental and *in silico* approaches based on quantum mechanics and classical molecular dynamics.[6] For instance, infrared (IR), ultrafast, and two-dimensional IR spectroscopy have provided high-resolution insights into their interconversion dynamics.[7–10] Ultrafast spectroscopy has directly observed proton hopping on femtosecond timescales, disentangling the role of HB fluctuations and collective solvent reorganization.[11,12] Neutron experiments have revealed the hydration arrangement of oxonium ions and their impact on the HB network,[13–15] while x-ray absorption[16,17] and scattering[18,19] experiments have elucidated the solvation dynamics and longer range ordering. *Ab initio* molecular dynamics (AIMD) and the advancement of neural network-enhanced simulations[20] have accurately modeled HB, proton transitions between different hydration configurations, or transfer mechanisms[21–25] and highlighted the influence of solvent polarization and nuclear quantum effects,[26,27] the coupling between hydration structures or transport properties of acid solutions,[28–30] and the acidification of air–water interfaces.[31–33] However, the accuracy of these studies depends on the choice of functionals, as significant deviations in condensed-phase thermodynamics persist even for pure water.[34] Alternatively, classical simulations[35] constitute a computationally efficient yet powerful approach to unveil key aspects of condensed matter. In modeling the oxonium cation, reducing computational cost—at the

expense of quantum effects like zero-point energy, tunneling, and the Grotthuss mechanism—can be mitigated using polarizable force fields[35–38] and explicitly incorporating proton transfer.[39–42] Despite ongoing progress in ion simulations,[42–44] challenges remain, particularly in polyatomic ions, regarding the selection and allocation of atomic charges (which is par for the course in the selection of the intermolecular potential parameters) and the intrinsic challenge of obtaining the appropriate potential energy and dipole moment surfaces.[45]

Consequently, the previously reported H_3O^+ force fields assign hydrogen partial charges ranging from $q_H \simeq 0.42e$–$1.26e$ (see collected data in Ref. 46), depending on the selected method handled for the charge assignment (recursive *trial-and-error* fitting[47,48] or quantum chemistry calculations[38,47,49,50]). Although the so-called ECC-ε approach provides an alternative to address this challenge,[51] we used the atomic dipole corrected Hirshfeld (ADCH) method,[52] which reduces basis set dependence and has proven effective for hydroxide anions.[53] The H_3O^+ geometry was optimized at the B3LYP/6-311++G(d,p) level with Gaussian16[54] and ADCH charge analysis using Multiwfn[55] yielded atomic charges of $-0.46403e$ (O) and $0.4881e$ (H). Electronic polarization effects[43] were incorporated via the electronic continuum correction.[56–61] Specifically, we adopted the Madrid-2019 model for electrolytes,[53,62–65] which is a combined TIP4P/2005 model for water.[66,67] The model employs Lennard-Jones interactions (parameters σ_{ij} and ε_{ij}) and electrostatic contributions (charges q_i) scaled by 0.85, ensuring agreement with bulk properties.[68–73] The set of self-Lennard-Jones σ_{ii} and ε_{ii} parameters of H_3O^+ are taken from the recent non-polarizable model reported in Ref. 46 for diluted (<1M) HCl solutions.

The fine-tuning of cross-interaction parameters is particularly significant here because, unlike in conventional electrolytes, an essential aspect of aqueous acid solutions is the shocking role of counterions that are no longer spectators but are involved in the persistent ion pairing observed in systems, such as hydrochloric acid[16,74–76] or nitric acid,[77–80] solutions, even in the low concentration regime. The subtle balance between the coexisting molecular (neutral, HA + H_2O), dissociated (A^- + H_3O^+), and ion-paired ($A^- \cdots H_3O^+$) limiting forms affects the solvation structure and dynamic behavior of oxonium ions in a concentration- and environment-dependent manner.[38,81,82] Here, the parameters between water and counterions were taken from the Madrid-2019 model.[62–64] The σ_{ij} and ε_{ij} parameters characterizing the cross water–H_3O^+ interactions are optimized employing the experimental densities of the solution as the target property (sacrificing other properties such as the hydration energies), and the Lorentz–Berthelot rule has been circumvented and modified à la carte for each interionic interaction to (i) minimize the difference between the experimental and simulated densities data and (ii) increase the number of contact ions pairs (CIPs) according to experimental evidence, at the time that precipitation is avoided close to the solubility limit (note that previous models have only studied acidic solutions up to 1.5 M[46]). The final parameters are collected in Table I.

Once the force field was optimized, we performed an intensive simulation survey to extract structural, thermodynamics, and transport properties of acidic solutions. Molecular dynamics calculations of densities and atom-to-atom structure were performed on a simulation box comprised of 555 TIP4P/2005 water molecules, and the necessary number of cations and anions to get the desired molality (i.e., the number of moles of solute per kilogram of solvent). Since molalities are experimentally determined from the number of moles of solute, H_3O^+ plays a double role as both solute and solvent (i.e., each HCl molecule subtracts one water molecule from the bulk, $HCl + H_2O \rightarrow Cl^- + H_3O^+$); in this case, molalities are re-scaled on account of this effect for a proper comparison with experimental data (see Table S1). We employed the isothermal–isobaric (NpT) ensemble at 1 bar using the GROMACS 4.6.7 package.[83] The equations of motion were integrated with the leapfrog algorithm[84] with a time step of 2 fs, and the temperature and pressure were kept constant employing the Nosé–Hoover thermostat[85,86] and the isotropic Parrinello–Rahman barostat,[87] respectively, both using a relaxation time of 2 ps. Given the C_{3v} symmetry of the oxonium ion, the SHAKE algorithm[88] was needed to impose the holonomic constraints. The oxonium cation was constructed following the data obtained by absorption spectroscopy[89] and Hartree–Fock calculations.[90] Particularly, the O–H and H–H distances were set to 0.980 and 1.619 Å, respectively, and the ∡HOH angle to 111.4°, thus ensuring a trigonal pyramidal shape. Unless otherwise mentioned, the cutoff of both the excluded volume and electrostatic interactions was 10 Å, the latter being treated within the particle mesh Ewald method.[91] Long-range corrections are applied for the Lennard-Jones contribution.

TABLE I. Coulombic and Lennard-Jones parameters of the H_3O^+ force field developed in this work. Partial charges $q_H = 0.414\,81e$, $q_O = -0.394\,42e$ were obtained by scaling values derived from the ADCH population method. The O–H bond distance in H_3O^+ was fixed at 0.98 Å and the ∡HOH angle to 111.4°. Subscripts w, ox, and n denote oxygen atoms from H_2O, H_3O^+, and NO_3^-, respectively. The parameters σ_{ij} and ε_{ij} are reported in units of Å and kJ mol^{-1}, respectively. We also indicate whether the Lorentz–Berthelot (LB) combining rule is applied or not (n-LB). The net charge of the oxonium cation is 0.85e in accordance with the Madrid-2019 force field.

Self-interaction parameters		
Parameter	Value	Source
q_O	$-0.394\,42e$	This work
q_H	$0.414\,81e$	This work
$\varepsilon_{O_{ox}-O_{ox}}$	0.800 00	From Ref. 46
$\sigma_{O_{ox}-O_{ox}}$	3.100 00	From Ref. 46
Cross-interaction parameters		
Parameter	Value	Mixing route
$\varepsilon_{O_{ox}-O_w}$	0.787 35	LB
$\varepsilon_{O_{ox}-Cl^-}$	0.248 00	LB
$\varepsilon_{O_{ox}-Br^-}$	0.300 39	LB
$\varepsilon_{O_{ox}-I^-}$	0.378 43	LB
$\varepsilon_{O_{ox}-N_n}$	0.754 19	LB
$\varepsilon_{O_{ox}-O_n}$	0.838 09	LB
$\sigma_{O_{ox}-O_w}$	2.800 00	n-LB
$\sigma_{O_{ox}-Cl^-}$	3.500 00	n-LB
$\sigma_{O_{ox}-Br^-}$	3.600 00	n-LB
$\sigma_{O_{ox}-I^-}$	3.700 00	n-LB
$\sigma_{O_{ox}-N_n}$	3.125 00	LB
$\sigma_{O_{ox}-O_n}$	3.450 00	n-LB

As previously mentioned, the target property used to adjust the model is the density of the aqueous solutions. In Fig. 1, we present a comparison between the experimental data (solid line) and the simulation results (symbols, see Table SIV) for the densities as a function of the molality for the selected acidic species, i.e., hydrogen halides, HX, with X = {Cl, Br, I}, and HNO_3. Consistently with previous studies, where we successfully described the experimental densities of more than 60 salts,[53,62–65] the results for acids follow a similar trend. We accurately reproduce the experimental densities of strong HX acids (with $pK_a^{HCl} = -6.3$[94], $pK_a^{HBr} = -9.0$ and $pK_a^{HI} = -9.5$[95]) and HNO_3 ($pK_a = -1.64$[96]), being the mean relative deviation of the simulated vs experimental data (defined as $\sum_i |1 - \rho_i^{exp}/\rho_i^{MD}|/N$) of 0.4%, 0.7%, 0.6%, and 0.4% for HCl, HBr, HI, and HNO_3, respectively. Whereas, in all cases, the global deviations are below 1%, the relative higher values found in the HBr and HI solutions were an expected drawback since it was previously reported that bromide and iodide ions pose a challenge for non-polarizable models.[97] Even though higher differences were found above this molality range, acid concentrations surpassing those correctly predicted by the present force field are of limited practical interest.

Next, we focused on the determination of the temperature of maximum in density (TMD) at 1 bar. Besides serving as a stringent test for assessing the transferability of the model in the supercooled region, the TMD (and the anomalies in other response functions) plays a crucial role in demonstrating the existence of a liquid–liquid critical point under deeply supercooled conditions,[105] which was predicted only by simulations[106,107] so far, but evidenced experimentally.[108,109] In this context, the TMD captures the modifications of the water tetrahydricity involved in the liquid–liquid transition[110,111] induced by dissolved ions and is gaining particular importance as a target property in the development of force fields.[67] Opportunely, the Madrid-2019 model has also been successfully tested against the TMD for several electrolyte solutions.[68,97,112] Here, following the same methodology, the density of supercooled HCl and HNO_3 solutions (0.98 *m*) for a number of temperatures has been evaluated [see Fig. 2(a)]. The raw simulation data (Table SV) were fitted to a cubic polynomial to determine the TMD analytically.

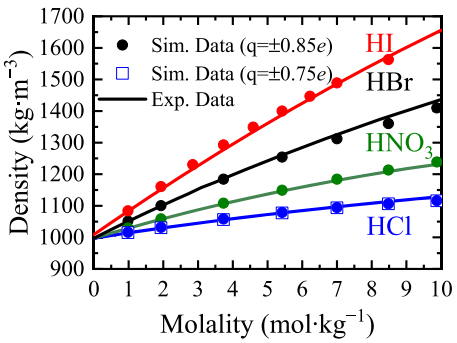

FIG. 1. Densities as a function of the molality for acidic solutions at 298.15 K and 1 bar. Full symbols represent the molecular dynamics results, while the continuous lines stand for the experimental data. Full circles stand for the Madrid-2019 model ($q = \pm 0.85e$). For HCl, we also considered a model with $q = \pm 0.75e$ represented with empty squares (the parameters for HCl and $q = \pm 0.75e$ are provided in the supplementary material). Experimental densities for all species but HI are those from Ref. 92. For HI, the values are obtained from a cubic polynomial fit to the experiments in Ref. 93. Error bars are smaller than the symbol size.

For comparison, we only found indirect experimental values of the TMD for the HCl solutions in the dated Ref. 104 (although no datum for the dependence of the density on the temperature is reported). The interpolation of the experiments to 0.98 *m* leads to $TMD_{HCl}^{exp} = 269.6$ K, in very good agreement with the simulations, from which $TMD_{HCl}^{MD} = 269.3$ K at the same molality. For diluted solutions, where the importance of interionic interactions is minor, the TMD shifts ($\Delta = TMD_{solution} - TMD_{water}$) are linear with *m*, i.e., $\Delta = K_m m$, with K_m being the specific Despretz constant of the electrolyte. K_m can be written in an additive or "group" approximation to extract limiting ion contributions, $K_m^{\pm}$, as $K_m = \nu_+ K_m^+ + \nu_- K_m^-$, with ν_+ and ν_- being the cation and anion stoichiometric coefficients, respectively.[99] Using the experimental K_m constants for Cl^- from Ref. 97, the contribution K_m^+ to the Despretz constant is $K_m^{H_3O^+} = -4.5$ K kg mol^{-1}. Note that a value of $K_m^{Li^+} = -3$ K kg mol^{-1} is the reference figure in our molality scale,[68] hampering a direct comparison with other reported values.[98,99] The molecular dynamics results for the $TMD_{HNO3}^{MD} = 259.1$ K, i.e., more than 5 K below the experimental $TMD_{HNO3}^{exp} \approx 264.2$ K.[98,99] This slightly larger deviation with respect to experiment is intrinsic to the NO_3^- model, as extensively discussed in Ref. 112. It is important to note that accurately modeling the TMD of electrolytes requires a water model that reproduces the correct TMD. For example, the SPC/E (Simple Point Charge/Extended) model predicts a TMD of 241 K,[113] i.e., 36 K lower than the experimental value.

We continue to study the viscosity coefficients of the solutions, computed using the Green–Kubo formalism, following the methodology outlined in Ref. 114. Briefly, the simulations involved a system consisting of 4440 water molecules along with the required number of ions for each concentration studied. Shortly, we perform a preliminary simulation of 20 ns in the *NpT* ensemble to calculate the average volume of the box, followed by a production run of 50 ns in the canonical (*NVT*) ensemble. In Fig. 2(b), we present the simulation (Table SVI) vs experimental viscosities of the solutions as a function of molality. The relatively smaller increase in viscosity when protons are added to water compared to equivalent standard electrolytes (i.e., HCl vs NaCl) has been ascribed to the screening effect of hydrogen–hydrogen repulsion between water molecules.[115] In the case of hydrogen halides, the simulation results (filled circles) overestimate the experimental values, but are only slightly underestimated for HNO_3.

Reproducing the viscosity coefficient of electrolyte solutions goes through a proper description of the structure of the system and the balance between the electrostatic and volumetric effects of the dissolved ions in the short- and long-range structure of the HB network of water.[116] In an attempt to disclose these points, we considered HCl and HNO_3[96] to expose the differential effects induced by atomic and polyatomic counteranions and of the acid strengths. The main structural features are plotted in Figs. 2(c) and 2(d) as extracted from atom-to-atom radial distribution functions (RDFs). Considering the HCl solutions first [Fig. 2(c)], the position of the first coordination shell of water (2.78 Å) agrees with that found for the TIP4P/2005 model[67] and remains unchanged with the acid concentration. However, the hydration number (HN) of water changed from 5 to 2 in the explored molality range, and the second peak, characteristic of the extended HB network, progressively shift-downs from ~4.4 to 3.8 Å at 9.88 *m*. Both the change in HN and the shrinkage were observed in Ref. 15. Similarly, the $O_{ox} \cdots O_w$

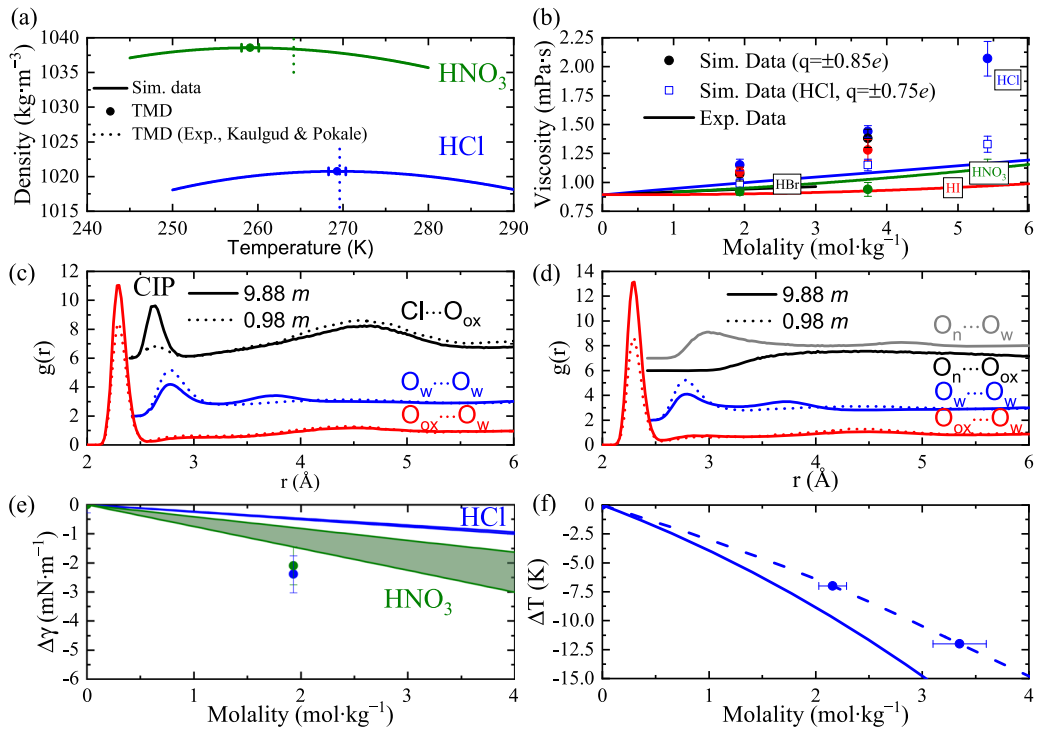

FIG. 2. (a) Densities as a function of temperature for 0.98 *m* acidic solutions of HCl (blue) and HNO3 (green) at 1 bar. Continuous lines stand for the third order polynomial fit to simulation data and full circles denote the TMD. Dotted vertical lines are the estimated experimental values from Refs. 98 and 99. See the main text for details. (b) Shear viscosities as a function of the electrolyte molality for acidic solutions at 298.15 K and 1 bar. Full symbols represent the molecular dynamics results, while the continuous lines stand for the experimental data. Full circles stand for the Madrid-2019 model ($q = \pm 0.85e$), while the HCl model with $q = \pm 0.75e$ is represented with empty squares. Experimental viscosities for HCl and HBr are taken Ref. 92. For HI, the values are obtained from a cubic polynomial fit to the experiments in Ref. 93. The viscosities of HNO_3 solutions were obtained from Ref. 100. (c) $Cl\cdots O_{ox}$, $O_w\cdots O_w$, and $O_{ox}\cdots O_w$ radial distribution functions of HCl solutions at low (0.98 *m*, dotted lines) and high (9.88 *m*, solid line) concentrations at 298.15 K and 1 bar. (d) $O_n\cdots O_{ox}$, $O_w\cdots O_w$, and $O_{ox}\cdots O_w$ radial distribution functions of HNO_3 solutions at low (0.98 *m*, dotted lines) and high (9.88 *m*, solid line) concentrations at 298.15 K and 1 bar. (e) Results for $\Delta\gamma$ for HCl and HNO_3 acidic solutions at 298.15 K. Full circles represent the molecular dynamics results, and the shaded area enclosed by the continuous lines corresponds to the $\Delta\gamma$ range extracted from the experimental data in Refs. 101–103. (f) Freezing point depression of HCl solutions at 1 bar. Continuous lines stand for experimental data in Ref. 104 and circles denote the molecular dynamics results. The dashed line is a guide to the eye.

RDF shows an intense and well-resolved peak at 2.30 Å, which corresponds to the water–H_3O^+ complex, although at the $O_{ox}\cdots O_w$ distance is slightly smaller than the experimental value.[15,16] However, it should be recognized that, at such short distances, interactions are largely governed by quantum mechanical effects akin to chemical bonding. These interactions cannot be accurately represented by classical force fields based solely on non-bonded Coulomb and van der Waals terms. The HN_{ox} is three as expected[35] and remains constant with the HCl concentration. This is fully consistent with the Eigen structure (i.e., an oxonium cation forming a hydrogen bond with three neighboring molecules of water). Since the force field proposed here does not include proton hopping, the potential contribution of Zundel structures (i.e., a proton located between two molecules of water) to transport and thermodynamic properties is not contemplated (see the Supplementary Material of Ref. 117 for a historical perspective on Eigen and Zundel ions and Ref. 118 for a dynamic view of the Eigen–Zundel interconversion).

The most striking feature highlighted in the literature is the appearance of contracted CIPs even at low HCl concentration. Here, the CIP is observed at the first peak of the $Cl\cdots H_{ox}$ and $Cl\cdots O_{ox}$ RDFs at 1.66 and 2.62 Å and experienced a 30-fold increase between the minimum and maximum HCl molalities, as observed in Ref. 28. The CIP is contracted (at shorter distances) compared to the hydration water of Cl^-, with $Cl\cdots O_w$ and $Cl\cdots O_{ox}$ distances of 3.05 and 2.63 Å, respectively, in agreement with the observations in Refs. 16 and 81 by ~0.2 Å. Note that the potential association of this peak with the presence of bihalogenide[19] (HX_2^-) anions or molecular HX would be inconsistent with our rigid model and has recently been disregarded.[75] Concomitant to the CIPs increment, the Cl^- anion progressively displaced one of its six bulk coordination water to H_3O^+, but keeping a sixfold coordination.[16] The structure found for HBr y HI is similar except for the counteranion size and the progressively smaller CIP value in HBr and HI, the former being consistent with Ref. 81 (see Fig. S1).

Provided the complex dependence of the local structure of HCl solutions nicely correlates with the experimental and *first principles* molecular dynamics studies, we explored electrostatic effects in a

twofold way. (I) In a first attempt, we used a box that mimicked an aqueous solution of HCl 1.98 m to calculate the shear viscosity of a number of models with different charge distributions (see Table SVII). It was found that the charge distribution obtained from the ADCH method provides the smallest deviation from the experimental data. (II) The long-range order effect on the HB arrangement was tested by developing a HCl model with ionic charges scaled by 0.75 in which the O_{ox}–O_w, O_{ox}–O_{ox}, and O_{ox}–Cl^- are optimized (see Tables SII and SIII), while H_2O–H_2O, H_2O–Cl^-, and Cl^-–I^- parameters are taken from the Madrid-transport model in Ref. 70. This selection accounts for the fact that the use of scaled charges improves the prediction of the viscosity and that for monovalent ions charges of ±0.75e have been found to be of particular success,[70,119] although for polyatomic ions the situation is less anticipable.[62,120] The agreement of the computational results (Tables SIV and SVI) with the experimental densities (0.5% on average) and viscosities is shown in Figs. 1 and 2(b), respectively. Such results are consistent with those reported in the so-called Madrid-transport model[70,119] and can be translated as "the higher the selected charge of an ion, the higher the viscosity." The price paid is an incorrect structure that is detrimental for other properties (such as the TMD that increases to 270.9 K, see Fig. S3) that seem to be dominated by the volumetric effect. In Fig. S2, we show that the HCl model of net charge 0.75e displays a less contracted $H_3O^+\cdots H_2O$ structure and a huge amount of CIPs compared to the Madrid-2019 model. Overall, to accurately model the viscosities of aqueous HX solutions, we recommend the use of the model with charges scaled by 0.75; however, as previously demonstrated, a model with charges of ±0.85e constitutes an "all purpose" solution to capture the wider range of properties of electrolyte solutions at a time.[70]

Some structural aspects are shared by HNO_3 solutions [see Fig. 2(d)]. For example, the downshift of the second peak of the $O_w\cdots O_w$ RDF or the decrease of the HN_w from 5 to 2. One of these depleted water molecules is replaced by a H_3O^+ cation, which is, in turn, coordinated with three water molecules. The position of the first clear maximum of the $O_n\cdots O_{ox}$ at ~3 Å agrees with that obtained from x-ray photoelectron spectroscopy and *ab initio* molecular dynamics in Ref. 77. However, no CIPs are detected at any concentration, but solvent-separated ion pairs. This is in contrast with recent AIMD-aided nuclear magnetic resonance experiments[78] and quantum chemical studies,[80,81] which concluded that given the "weakness" of the acid, HNO_3, and/or contracted CIPs are present in the solutions. Furthermore, although the mean $HN_{NO_3^-}$ ~ 15 agrees with reliable experiments, some aspects of the local structure and the complex hydration of NO_3^- (reviewed and discussed in the context of the Madrid-2019 model in Ref. 64) are missing in the model, as advertised in Ref. 112. Hence, the effect of electrostatic perturbation of the H_3O^+ in the HB network (and viscosity) is compensated for by the strong local effects entailed by the complex hydration of the HNO_3 and NO_3^- species and the absence of neutral HNO_3 (not explicitly defined in the model) or paired ions (not found during simulations).

Finally, the consequences of all these effects on the coexistence properties for surface tension (γ) and freezing point depression are analyzed. The surface tension was evaluated in the *NVT* ensemble using the virial approach as in Ref. 70. Briefly, a system of 4440 water molecules and the corresponding number of ions are placed in contact with water vapor in an elongated box ($L_x = L_y \approx 3L_z$), in which the cutoff was set to 1.4 nm. The surface tension of acidic electrolytes exhibited a negative slope ($d\gamma/dm < 0$) with increasing molality, compatible with H_3O^+ adsorption at the surface. This trend was qualitatively reproduced by our model (see Table VIII), as shown in Fig. 2(e), and is consistent with the experimental data[101–103] for $\Delta\gamma = \gamma - \gamma_0$, where γ_0 represents the surface tension of pure water. The observed deviations were of a magnitude similar to that reported in a recent AIMD study,[122] but noticeably smaller for HNO_3. Interestingly, this result is counterintuitive with the known behavior of HNO_3 and HCl at the interface: HNO_3 remains predominantly undissociated,[123] while HCl is highly dissociated.[81,124] This highlights the critical role of counterion interactions in partially dissociating electrolytes, as these interactions significantly influence the properties of acidic solutions, with surface tension being no exception.[81]

Finally, the freezing point depression at different molalities, $\Delta T = T_f^{sol} - T_f^w$ (T_f^w being the freezing point of pure water and T_f^{sol} being the freezing point of the solution) was determined for HCl solutions with the direct coexistence method (see Ref. 73 for further details) at room pressure. Briefly, the secondary prismatic plane $(1\bar{2}10)$ of a slab (2048 molecules) of ice I_h was in contact with aqueous HCl solutions ~1.8 m (65 × 2 ions and 2000 water molecules). The simulations run for 1 μs for equilibration and 1 μs for production. In Fig. 2(f), the experimental values from Ref. 104 are presented together with molecular dynamics data (see Table IX). Similar deviations to those reported previously for the Madrid-2019 model were found in Ref. 73. As discussed by these authors, the difference in the melting temperature of between the TIP4P/2005[113] and experiment (250 vs 273 K) along with the difference also observed for the melting enthalpy is responsible for some deviations found in the freezing point depression curve. A new route to reduce this difference has been recently investigated in Ref. 125 by combining the Madrid-2019 force field with the TIP4P/Ice model of water[126] (which predicts better melting temperature and enthalpy in comparison with the TIP4P/2005).

To conclude, we compare the effects of acids (H_3O^+ cation) and bases (OH^- anion) on various properties of aqueous solutions, which are of particular interest from both a fundamental and practical perspective. Figures 3(a)–3(d) present the experimental results alongside simulations performed using the Madrid-2019 force field, which was recently extended to include OH^-, as well as the force field developed in this work for H_3O^+. Specifically, this comparison includes viscosity, Δ, $\Delta\gamma$, and freezing point depression. In general, for the same concentration, OH^- has a stronger influence on the solution properties than H_3O^+. For example, the shift in the temperature of maximum density (TMD) is more pronounced for bases, with the Despretz constant for H_3O^+ being approximately half of that corresponding to OH^- ($K_m^{OH^-}$)[53] [Fig. 3(a)]. Similarly, viscosity increases significantly in the presence of bases compared to acids [Fig. 3(b)]. The behavior of surface tension also shows significant differences: NaOH exhibits negative adsorption, leading to an increase in surface tension, whereas HCl shows positive adsorption, causing a decrease [Fig. 3(c)]. Interestingly, the only exception to this trend is found in freezing point depression, where acids appear to be more effective; for the same concentration, HCl induces a greater decrease in freezing temperature than NaOH [Fig. 3(d)]. Although

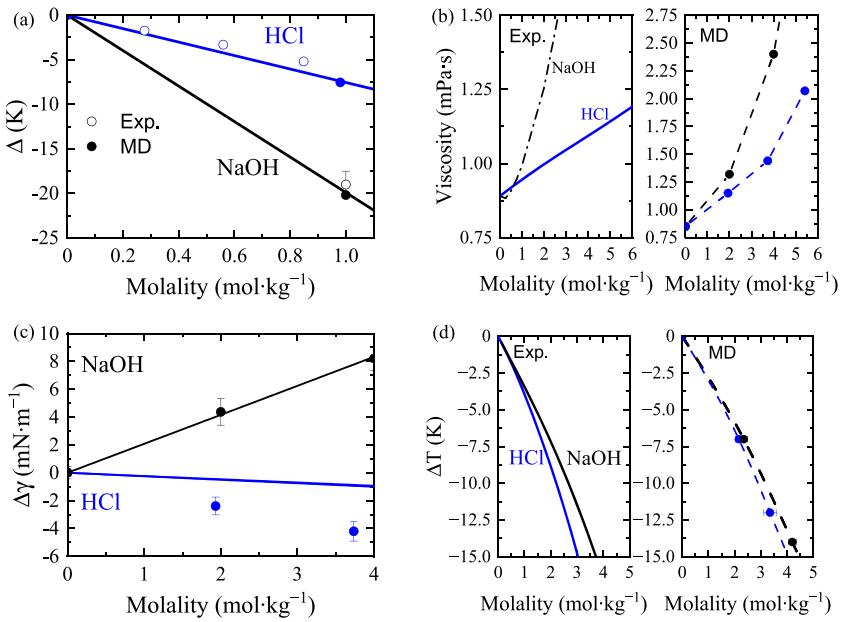

FIG. 3. (a) Experimental trend (empty symbols) of Δ for NaOH[53] and HCl.[104] Molecular dynamics results are plotted as full symbols, and the continuous line is a guide to the eye. (b) Experimental (left) and simulated (right) shear viscosities as a function of the electrolyte molality for HCl and NaOH solutions. Experimental data obtained from Ref. 121 and simulation points from Refs. 53 and 69 for NaCl and NaOH, respectively. The dashed lines in the right panel are a guide to the eye. (c) Comparison between the surface behavior of NaOH and HCl. $\Delta\gamma$ range extracted from the experimental data in Refs. 101–103 and from Ref. 53 for NaOH simulations. (d) Freezing point depression of HCl and NaOH solutions. The left panel shows experimental data in Ref. 104. Molecular dynamics results for NaOH are reported in Ref. 53. The dashed lines are a guide to the eye. Thermodynamic conditions as in Fig. 2 [panels (a), (b), (e), and (f)].

the model does not quantitatively reproduce all experimental results with complete accuracy, it provides a qualitative description of viscosity and a semi-quantitative agreement for TMD, surface tension, and freezing point depression. Moreover, it correctly captures the experimental trends and the differences in how acids and bases influence the properties of water.

To sum up, this study presents an optimized classical force field for the oxonium ion within the Madrid-2019 framework. The model accurately reproduces key thermodynamic properties of acidic solutions, such as density and the temperature of maximum density, across a wide range of acid concentrations, including HCl, HBr, HI, and HNO_3. Notably, it is the first force field to simulate concentrations as high as 10 *m*. It balances computational efficiency and accuracy by employing scaled charges and charge distributions derived using the ADCH method. While the model shows strong agreement with experimental data for structural and thermodynamic properties in most practical scenarios (acid concentration below 1 *m*), it has limitations. Specifically, (i) it struggles to capture ion-pairing leading to neutral molecules, which could significantly affect transport and surface properties at high concentrations, and (ii) it cannot fully describe properties, such as electrical conductivity and oxonium ion diffusion, which require a quantum-level treatment of the Grotthuss mechanism. Despite these challenges, the force field provides a robust platform for studying key physicochemical aspects of aqueous acid solutions. In addition, the findings presented here highlight critical challenges for advancing molecular modeling strategies. With the incorporation of H_3O^+ and OH^-, the Madrid-2019 force field can now simulate up to 76 different electrolyte solutions by combining 11 cations (alkali metals, alkaline earth metals, NH_4^+, and H_3O^+) and seven anions (halides, NO_3^-, SO_4^{2-}, and OH^-), as well as numerous multicomponent systems. Future developments explicitly account for neutral molecular forms, such as non-dissociated gaseous HCl.

SUPPLEMENTARY MATERIAL

The supplementary material encompasses supporting.pdf: raw simulated data for densities, viscosities, surface tension, and temperature of maximum in density; representative site-site radial distribution functions; TMD data for the HCl model with $q = \pm 0.75e$; *Topology* file for GROMACS with optimized potential parameters of H_3O^+; and *Topology* file for GROMACS with optimized potential parameters of HCl with $q = \pm 0.75e$.

ACKNOWLEDGMENTS

This work was funded by Grant No. PID2022-136919NB-C31 and PID2022-136919NA-C33 of the Ministry of Science, Innovation and Universities MCIN/AEI/10.13039/501100011033. S.B. acknowledges Ayuntamiento de Madrid for a Residencia de Estudiantes grant. The authors were deeply grateful to J. R. Avilés-Moreno for introducing them to the ADCH method.

AUTHOR DECLARATIONS

Conflict of Interest

The authors have no conflicts to disclose.

Author Contributions

S. Blazquez and M. de Lucas contributed equally to this work.

S. Blazquez: Data curation (equal); Formal analysis (equal); Investigation (equal); Validation (equal); Writing – original draft

(equal). **M. de Lucas**: Data curation (equal); Formal analysis (equal); Investigation (equal); Validation (equal); Writing – original draft (equal). **C. Vega**: Conceptualization (equal); Funding acquisition (equal); Methodology (equal); Supervision (equal); Writing – original draft (equal). **F. Gámez**: Conceptualization (equal); Data curation (equal); Funding acquisition (equal); Supervision (lead); Writing – original draft (equal); Writing – review & editing (lead).

DATA AVAILABILITY

The data that support the findings of this study are available within the article and its supplementary material.

REFERENCES

[1]N. Agmon, "The Grotthuss mechanism," Chem. Phys. Lett. **244**(5–6), 456–462 (1995).
[2]D.-W. Lim and H. Kitagawa, "Proton transport in metal–organic frameworks," Chem. Rev. **120**(16), 8416–8467 (2020).
[3]S. Fop, "Solid oxide proton conductors beyond perovskites," J. Mater. Chem. A **9**(35), 18836–18856 (2021).
[4]X.-M. Li, J. Jia, D. Yang, J. Jin, and J. Gao, "Construction of biomimetic proton transport channels in metal-organic framework," Chin. Chem. Lett. **35**(3), 108474 (2024).
[5]M. Pan, C. Pan, C. Li, and J. Zhao, "A review of membranes in proton exchange membrane fuel cells: Transport phenomena, performance and durability," Renewable Sustainable Energy Rev. **141**, 110771 (2021).
[6]N. Agmon, H. J. Bakker, R. K. Campen, R. H. Henchman, P. Pohl, S. Roke, M. Thämer, and A. Hassanali, "Protons and hydroxide ions in aqueous systems," Chem. Rev. **116**(13), 7642–7672 (2016).
[7]M. Śmiechowski and J. Stangret, "Proton hydration in aqueous solution: Fourier transform infrared studies of HDO spectra," J. Chem. Phys. **125**(20), 204508 (2006).
[8]K. Mizuse, A. Fujii, and N. Mikami, "Long range influence of an excess proton on the architecture of the hydrogen bond network in large-sized water clusters," J. Chem. Phys. **126**(23), 231101 (2007).
[9]S. T. Roberts, K. Ramasesha, P. B. Petersen, A. Mandal, and A. Tokmakoff, "Proton transfer in concentrated aqueous hydroxide visualized using ultrafast infrared spectroscopy," J. Phys. Chem. A **115**(16), 3957–3972 (2011).
[10]W. B. Carpenter, Q. Yu, J. H. Hack, B. Dereka, J. M. Bowman, and A. Tokmakoff, "Decoding the 2D IR spectrum of the aqueous proton with high-level VSCF/VCI calculations," J. Chem. Phys. **153**(12), 124506 (2020).
[11]S. F. Sutton, C. H. Rotteger, C. K. Jarman, P. Tarakeshwar, and S. G. Sayres, "Ultrafast proton transfer and contact ion-pair formation in formic acid clusters," J. Phys. Chem. Lett. **14**(37), 8306–8311 (2023).
[12]W. B. Carpenter, N. H. C. Lewis, J. A. Fournier, and A. Tokmakoff, "Entropic barriers in the kinetics of aqueous proton transfer," J. Chem. Phys. **151**(3), 034501 (2019).
[13]A. Botti, F. Bruni, M. A. Ricci, and A. K. Soper, "Eigen versus Zundel complexes in HCl-water mixtures," J. Chem. Phys. **125**(1), 014508 (2006).
[14]R. Mancinelli, A. Sodo, F. Bruni, M. A. Ricci, and A. K. Soper, "Influence of concentration and anion size on hydration of H^+ ions and water structure," J. Phys. Chem. B **113**(13), 4075–4081 (2009).
[15]A. Botti, F. Bruni, S. Imberti, M. A. Ricci, and A. K. Soper, "Ions in water: The microscopic structure of a concentrated HCl solution," J. Chem. Phys. **121**(16), 7840–7848 (2004).
[16]J. L. Fulton and M. Balasubramanian, "Structure of hydronium (H_3O^+)/chloride (Cl^-) contact ion pairs in aqueous hydrochloric acid solution: A Zundel-like local configuration," J. Am. Chem. Soc. **132**(36), 12597–12604 (2010).
[17]M. Cavalleri, L.-Å. Näslund, D. C. Edwards, P. Wernet, H. Ogasawara, S. Myneni, L. Ojamäe, M. Odelius, A. Nilsson, and L. G. M. Pettersson, "The local structure of protonated water from x-ray absorption and density functional theory," J. Chem. Phys. **124**(19), 194508 (2006).
[18]Y. Kameda, T. Usuki, and O. Uemura, "Diffraction studies on concentrated aqueous hydrochloric acid solutions," Isr. J. Chem. **39**(3–4), 283–289 (1999).
[19]N. Agmon, "Structure of concentrated HCl solutions," J. Phys. Chem. A **102**(1), 192–199 (1998).
[20]J. Behler, "First principles neural network potentials for reactive simulations of large molecular and condensed systems," Angew. Chem., Int. Ed. **56**(42), 12828–12840 (2017).
[21]M. Tuckerman, K. Laasonen, M. Sprik, and M. Parrinello, "*Ab initio* molecular dynamics of the solvation and transport of H_3O^+ and OH^- ions in water," J. Phys. Chem. **99**(16), 5749–5752 (1995).
[22]D. Marx, M. E. Tuckerman, J. Hutter, and M. Parrinello, "The nature of the hydrated excess proton in water," Nature **397**(6720), 601–604 (1999).
[23]A. Hassanali, F. Giberti, J. Cuny, T. D. Kühne, and M. Parrinello, "Proton transfer through the water gossamer," Proc. Natl. Acad. Sci. U. S. A. **110**(34), 13723–13728 (2013).
[24]Z. Zhu, A. P. Sokolov, and S. J. Paddison, "Proton transport mechanisms in aqueous acids: Insights from *ab initio* molecular dynamics simulations," J. Chem. Phys. **161**(15), 154504 (2024).
[25]A. Gomez, W. H. Thompson, and D. Laage, "Neural-network-based molecular dynamics simulations reveal that proton transport in water is doubly gated by sequential hydrogen-bond exchange," Nat. Chem. **16**(11), 1838–1844 (2024).
[26]G. Cassone, "Nuclear quantum effects largely influence molecular dissociation and proton transfer in liquid water under an electric field," J. Phys. Chem. Lett. **11**(21), 8983–8988 (2020).
[27]D. Marx, M. E. Tuckerman, and M. Parrinello, "Solvated excess protons in water: Quantum effects on the hydration structure," J. Phys.: Condens. Matter **12**(8A), A153 (2000).
[28]P. B. Calio, C. Li, and G. A. Voth, "Molecular origins of the barriers to proton transport in acidic aqueous solutions," J. Phys. Chem. B **124**(40), 8868–8876 (2020).
[29]M. de la Puente, A. Gomez, and D. Laage, "Neural network-based sum-frequency generation spectra of pure and acidified water interfaces with air," J. Phys. Chem. Lett. **15**(11), 3096–3102 (2024).
[30]D. Muñoz-Santiburcio, "Accurate diffusion coefficients of the excess proton and hydroxide in water via extensive *ab initio* simulations with different schemes," J. Chem. Phys. **157**(2), 024504 (2022).
[31]M. Flór, D. M. Wilkins, M. de la Puente, D. Laage, G. Cassone, A. Hassanali, and S. Roke, "Dissecting the hydrogen bond network of water: Charge transfer and nuclear quantum effects," Science **386**(6726), eads4369 (2024).
[32]M. de la Puente and D. Laage, "How the acidity of water droplets and films is controlled by the air–water interface," J. Am. Chem. Soc. **145**(46), 25186–25194 (2023).
[33]M. de la Puente, R. David, A. Gomez, and D. Laage, "Acids at the edge: Why nitric and formic acid dissociations at air–water interfaces depend on depth and on interface specific area," J. Am. Chem. Soc. **144**(23), 10524–10529 (2022).
[34]P. Montero de Hijes, C. Dellago, R. Jinnouchi, and G. Kresse, "Density isobar of water and melting temperature of ice: Assessing common density functionals," J. Chem. Phys. **161**(13), 131102 (2024).
[35]S. Roy and L. X. Dang, "Water exchange dynamics around H_3O^+ and OH^- ions," Chem. Phys. Lett. **628**, 30–34 (2015).
[36]W. Zhang and A. C. T. van Duin, "Second-generation ReaxFF water force field: Improvements in the description of water density and OH-anion diffusion," J. Phys. Chem. B **121**, 6021–6032 (2017).
[37]R. Vácha, D. Horinek, M. L. Berkowitz, and P. Jungwirth, "Hydronium and hydroxide at the interface between water and hydrophobic media," Phys. Chem. Chem. Phys. **10**(32), 4975–4980 (2008).
[38]J. S. Hub, M. G. Wolf, C. Caleman, P. J. van Maaren, G. Groenhof, and D. van der Spoel, "Thermodynamics of hydronium and hydroxide surface solvation," Chem. Sci. **5**(5), 1745–1749 (2014).
[39]M. G. Wolf and G. Groenhof, "Explicit proton transfer in classical molecular dynamics simulations," J. Comput. Chem. **35**(8), 657–671 (2014).
[40]A. Asthana and D. R. Wheeler, "A polarizable reactive force field for water to enable molecular dynamics simulations of proton transport," J. Chem. Phys. **138**(17), 174502 (2013).

[41] M. A. Lill and V. Helms, "Molecular dynamics simulation of proton transport with quantum mechanically derived proton hopping rates (Q-HOP MD)," J. Chem. Phys. **115**(17), 7993–8005 (2001).
[42] J. Xu, Y. Zhang, and G. A. Voth, "Infrared spectrum of the hydrated proton in water," J. Phys. Chem. Lett. **2**(2), 81–86 (2011).
[43] W. R. Smith, I. Nezbeda, J. Kolafa, and F. Moučka, "Recent progress in the molecular simulation of thermodynamic properties of aqueous electrolyte solutions," Fluid Phase Equilib. **466**, 19–30 (2018).
[44] P. Loche, P. Steinbrunner, S. Friedowitz, R. R. Netz, and D. J. Bonthuis, "Transferable ion force fields in water from a simultaneous optimization of ion solvation and ion–ion interaction," J. Phys. Chem. B **125**(30), 8581–8587 (2021).
[45] C. Vega, "Water: One molecule, two surfaces, one mistake," Mol. Phys. **113**(9–10), 1145–1163 (2015).
[46] D. J. Bonthuis, S. I. Mamatkulov, and R. R. Netz, "Optimization of classical nonpolarizable force fields for OH^- and H_3O^+," J. Chem. Phys. **144**(10), 104503 (2016).
[47] B. Temelso, T. Köddermann, K. N. Kirschner, K. Klein, and G. C. Shields, "Structure and thermodynamics of H_3O^+ $(H_2O)_8$ clusters: A combined molecular dynamics and quantum mechanics approach," Comput. Theor. Chem. **1021**, 240–248 (2013).
[48] I. Kusaka, Z.-G. Wang, and J. H. Seinfeld, "Binary nucleation of sulfuric acid-water: Monte Carlo simulation," J. Chem. Phys. **108**(16), 6829–6848 (1998).
[49] W. Chen, J. A. Wallace, Z. Yue, and J. K. Shen, "Introducing titratable water to all-atom molecular dynamics at constant pH," Biophys. J. **105**(4), L15–L17 (2013).
[50] R. Vácha, V. Buch, A. Milet, J. P. Devlin, and P. Jungwirth, "Autoionization at the surface of neat water: Is the top layer pH neutral, basic, or acidic?," Phys. Chem. Chem. Phys. **9**(34), 4736–4747 (2007).
[51] M. Předota and D. Biriukov, "Electronic continuum correction without scaled charges," J. Mol. Liq. **314**, 113571 (2020).
[52] T. Lu and F. Chen, "Atomic dipole moment corrected Hirshfeld population method," J. Theor. Comput. Chem. **11**(01), 163–183 (2012).
[53] M. de Lucas, S. Blazquez, J. Troncoso, C. Vega, and F. Gámez, "Dressing a non-polarizable force field for OH^- in TIP4P/2005 aqueous solutions with corrected Hirshfeld charges," J. Phys. Chem. Lett. **15**(37), 9411–9418 (2024).
[54] M. J. Frisch, G. W. Trucks, H. B. Schlegel, G. E. Scuseria, M. A. Robb, J. R. Cheeseman, G. Scalmani, V. Barone, G. A. Petersson, H. Nakatsuji, X. Li, M. Caricato, A. V. Marenich, J. Bloino, B. G. Janesko, R. Gomperts, B. Mennucci, H. P. Hratchian, J. V. Ortiz, A. F. Izmaylov, J. L. Sonnenberg, D. Williams-Young, F. Ding, F. Lipparini, F. Egidi, J. Goings, B. Peng, A. Petrone, T. Henderson, D. Ranasinghe, V. G. Zakrzewski, J. Gao, N. Rega, G. Zheng, W. Liang, M. Hada, M. Ehara, K. Toyota, R. Fukuda, J. Hasegawa, M. Ishida, T. Nakajima, Y. Honda, O. Kitao, H. Nakai, T. Vreven, K. Throssell, J. A. Montgomery, Jr., J. E. Peralta, F. Ogliaro, M. J. Bearpark, J. J. Heyd, E. N. Brothers, K. N. Kudin, V. N. Staroverov, T. A. Keith, R. Kobayashi, J. Normand, K. Raghavachari, A. P. Rendell, J. C. Burant, S. S. Iyengar, J. Tomasi, M. Cossi, J. M. Millam, M. Klene, C. Adamo, R. Cammi, J. W. Ochterski, R. L. Martin, K. Morokuma, O. Farkas, J. B. Foresman, and D. J. Fox, Gaussian 16 Revision C.01, Gaussian, Inc., Wallingford, CT, 2016.
[55] T. Lu and F. Chen, "Multiwfn: A multifunctional wavefunction analyzer," J. Comput. Chem. **33**(5), 580–592 (2012).
[56] I. V. Leontyev and A. A. Stuchebrukhov, "Electronic continuum model for molecular dynamics simulations," J. Chem. Phys. **130**(8), 085103 (2009).
[57] I. V. Leontyev and A. A. Stuchebrukhov, "Electronic polarizability and the effective pair potentials of water," J. Chem. Theory Comput. **6**(10), 3153–3161 (2010).
[58] I. V. Leontyev and A. A. Stuchebrukhov, "Electronic continuum model for molecular dynamics simulations of biological molecules," J. Chem. Theory Comput. **6**(5), 1498–1508 (2010).
[59] I. Leontyev and A. Stuchebrukhov, "Accounting for electronic polarization in non-polarizable force fields," Phys. Chem. Chem. Phys. **13**, 2613–2626 (2011).
[60] I. V. Leontyev and A. A. Stuchebrukhov, "Polarizable mean-field model of water for biological simulations with AMBER and CHARMM force fields," J. Chem. Theory Comput. **8**(9), 3207–3216 (2012).
[61] I. V. Leontyev and A. A. Stuchebrukhov, "Polarizable molecular interactions in condensed phase and their equivalent nonpolarizable models," J. Chem. Phys. **141**(1), 014103 (2014).
[62] I. M. Zeron, J. L. F. Abascal, and C. Vega, "A force field of Li^+, Na^+, K^+, Mg^{2+}, Ca^{2+}, Cl^-, and SO_4^{2-} in aqueous solution based on the TIP4P/2005 water model and scaled charges for the ions," J. Chem. Phys. **151**, 134504–134516 (2019).
[63] S. Blazquez, M. M. Conde, J. L. F. Abascal, and C. Vega, "The Madrid-2019 force field for electrolytes in water using TIP4P/2005 and scaled charges: Extension to the ions F^-, Br^-, I^-, Rb^+, and Cs^+," J. Chem. Phys. **156**, 044505 (2022).
[64] V. M. Trejos, M. de Lucas, C. Vega, S. Blazquez, and F. Gámez, "Further extension of the Madrid-2019 force field: Parametrization of nitrate (NO_3^-) and ammonium (NH_4^+) ions," J. Chem. Phys. **159**(22), 224501 (2023).
[65] S. Blazquez, I. C. Bourg, and C. Vega, "Madrid-2019 force field: An extension to divalent cations Sr^{2+} and Ba^{2+}," J. Chem. Phys. **160**(4), 046101 (2024).
[66] J. L. F. Abascal and C. Vega, "A general purpose model for the condensed phases of water: TIP4P/2005," J. Chem. Phys. **123**, 234505 (2005).
[67] L. F. Sedano, S. Blazquez, and C. Vega, "Accuracy limit of non-polarizable four-point water models: TIP4P/2005 vs OPC. Should water models reproduce the experimental dielectric constant?," J. Chem. Phys. **161**(4), 044505 (2024).
[68] L. F. Sedano, S. Blazquez, E. G. Noya, C. Vega, and J. Troncoso, "Maximum in density of electrolyte solutions: Learning about ion–water interactions and testing the Madrid-2019 force field," J. Chem. Phys. **156**, 154502 (2022).
[69] S. Blazquez, I. M. Zeron, M. M. Conde, J. L. F. Abascal, and C. Vega, "Scaled charges at work: Salting out and interfacial tension of methane with electrolyte solutions from computer simulations," Fluid Phase Equilib. **513**, 112548 (2020).
[70] S. Blazquez, M. M. Conde, and C. Vega, "Scaled charges for ions: An improvement but not the final word for modeling electrolytes in water," J. Chem. Phys. **158**(5), 054505 (2023).
[71] S. Blazquez, C. Vega, and M. M. Conde, "Three phase equilibria of the methane hydrate in NaCl solutions: A simulation study," J. Mol. Liq. **383**, 122031 (2023).
[72] S. Blazquez, M. M. Conde, and C. Vega, "Solubility of CO_2 in salty water: Adsorption, interfacial tension and salting out effect," Mol. Phys. **122**, e2306242 (2024).
[73] C. P. Lamas, C. Vega, and E. G. Noya, "Freezing point depression of salt aqueous solutions using the Madrid-2019 model," J. Chem. Phys. **156**(13), 134503 (2022).
[74] L. Kazmierczak, I. Janik, M. Wolszczak, and D. Swiatla-Wojcik, "Dynamics of ion pairing in dilute aqueous HCl solutions by spectroscopic measurements of hydroxyl radical conversion into dichloride radical anions," J. Phys. Chem. B **125**(33), 9564–9571 (2021).
[75] M. D. Baer, J. L. Fulton, M. Balasubramanian, G. K. Schenter, and C. J. Mundy, "Persistent ion pairing in aqueous hydrochloric acid," J. Phys. Chem. B **118**(26), 7211–7220 (2014).
[76] J. Xu, S. Izvekov, and G. A. Voth, "Structure and dynamics of concentrated hydrochloric acid solutions," J. Phys. Chem. B **114**(29), 9555–9562 (2010).
[77] T. Lewis, B. Winter, A. C. Stern, M. D. Baer, C. J. Mundy, D. J. Tobias, and J. C. Hemminger, "Dissociation of strong acid revisited: X-ray photoelectron spectroscopy and molecular dynamics simulations of HNO_3 in water," J. Phys. Chem. B **115**(30), 9445–9451 (2011).
[78] I. Munar, M. Ö. Özer, E. Fusco, D. Uner, V. Aviyente, and M. Bühl, "Dissociation of HNO_3 in water revisited: Experiment and theory," Phys. Chem. Chem. Phys. **26**(23), 16616–16624 (2024).
[79] N. H. C. Lewis, J. A. Fournier, W. B. Carpenter, and A. Tokmakoff, "Direct observation of ion pairing in aqueous nitric acid using 2D infrared spectroscopy," J. Phys. Chem. B **123**(1), 225–238 (2018).
[80] J. R. Scott and J. B. Wright, "Computational investigation of the solvation of nitric acid: Formation of the NO_3^- and H_3O^+ ion pair," J. Phys. Chem. A **108**(47), 10578–10585 (2004).
[81] M. D. Baer, D. J. Tobias, and C. J. Mundy, "Investigation of interfacial and bulk dissociation of HBr, HCl, and HNO_3 using density functional theory-based molecular dynamics simulations," J. Phys. Chem. C **118**(50), 29412–29420 (2014).
[82] M. G. Wolf, H. Grubmüller, and G. Groenhof, "Anomalous surface diffusion of protons on lipid membranes," Biophys. J. **107**(1), 76–87 (2014).
[83] B. Hess, C. Kutzner, D. van der Spoel, and E. Lindahl, "GROMACS 4: Algorithms for highly efficient, load-balanced, and scalable molecular simulation," J. Chem. Theory Comput. **4**, 435–447 (2008).
[84] D. Beeman, "Some multistep methods for use in molecular dynamics calculations," J. Comput. Phys. **20**(2), 130–139 (1976).

[85]S. Nosé, "A molecular dynamics method for simulations in the canonical ensemble," Mol. Phys. **52**(2), 255–268 (1984).
[86]W. G. Hoover, "Canonical dynamics: Equilibrium phase-space distributions," Phys. Rev. A **31**, 1695–1697 (1985).
[87]M. Parrinello and A. Rahman, "Polymorphic transitions in single crystals: A new molecular dynamics method," J. Appl. Phys. **52**, 7182–7190 (1981).
[88]J. Ryckaert, G. C. Herman, and J. C. Berendsen, "Numerical integration of the cartesian equations of motion of a system with constraints: Molecular dynamics of *n*-alkanes," J. Comput. Phys. **23**(3), 327–341 (1977).
[89]T. J. Sears, P. R. Bunker, P. B. Davies, S. A. Johnson, and V. Špirko, "Diode laser absorption spectroscopy of D_3O^+: Determination of the equilibrium structure and potential function of the oxonium ion," J. Chem. Phys. **83**(6), 2676–2685 (1985).
[90]P. A. Kollman and C. F. Bender, "The structure of the H_3O^+ (hydronium) ion," Chem. Phys. Lett. **21**(2), 271–274 (1973).
[91]U. Essmann, L. Perera, M. L. Berkowitz, T. Darden, H. Lee, and L. G. Pedersen, "A smooth particle mesh Ewald method," J. Chem. Phys. **103**, 8577–8593 (1995).
[92]M. Laliberté, "A model for calculating the heat capacity of aqueous solutions, with updated density and viscosity data," J. Chem. Eng. Data **54**(6), 1725–1760 (2009).
[93]E. Nishikata, T. Ishii, and T. Ohta, "Viscosities of aqueous hydrochloric acid solutions, and densities and viscosities of aqueous hydroiodic acid solutions," J. Chem. Eng. Data **26**(3), 254–256 (1981).
[94]R. A. Robinson and R. G. Bates, "Dissociation constant of hydrochloric acid from partial vapor pressures over hydrogen chloride-lithium chloride solutions," Anal. Chem. **43**(7), 969–970 (1971).
[95]D. M. Petković, "Dissociation of strong acids in aqueous solutions," J. Chem. Soc., Dalton Trans. **1982**(12), 2425–2427.
[96]C. E. Housecroft and A. G. Sharpe, *Inorganic Chemistry* (Pearson Education, 2008), Vol. 1.
[97]F. Gámez, L. F. Sedano, S. Blazquez, J. Troncoso, and C. Vega, "Building a Hofmeister-like series for the maximum in density temperature of aqueous electrolyte solutions," J. Mol. Liq. **377**, 121433 (2023).
[98]T. Wakabayashi and K. Takaizumi, "Despretz constants for individual ions," Bull. Chem. Soc. Jpn. **55**, 3073–3078 (1982).
[99]M. V. Kaulgud and W. K. Pokale, "Measurement of the temperature of maximum density of aqueous solutions of some salts and acids," J. Chem. Soc., Faraday Trans. **91**(6), 999–1004 (1995).
[100]W. R. Bousfield, "CXCIV.—The study of the density and viscosity of aqueous solutions, with special reference to nitric acid. Part II. Viscosities," J. Chem. Soc., Trans. **107**, 1781–1797 (1915).
[101]P. K. Weissenborn and R. J. Pugh, "Surface tension of aqueous solutions of electrolytes: Relationship with ion hydration, oxygen solubility, and bubble coalescence," J. Colloid Interface Sci. **184**(2), 550–563 (1996).
[102]C. L. Henry, C. N. Dalton, L. Scruton, and V. S. J. Craig, "Ion-specific coalescence of bubbles in mixed electrolyte solutions," J. Phys. Chem. C **111**(2), 1015–1023 (2007).
[103]A. A. Abramzon and R. D. Gaukhberg, "Surface tension of salt solutions," Zh. Prikladnoj Khim. **66**(6), 1428–1438 (1993).
[104]E. W. Washburn, *International Critical Tables of Numerical Data, Physics, Chemistry and Technology: Vol. III* (McGraw Hill, New York, 1928).
[105]P. Gallo, K. Amann-Winkel, C. A. Angell, M. A. Anisimov, F. Caupin, C. Chakravarty, E. Lascaris, T. Loerting, A. Z. Panagiotopoulos, J. Russo, J. A. Sellberg, H. E. Stanley, H. Tanaka, C. Vega, L. Xu, and L. G. M. Pettersson, "Water: A tale of two liquids," Chem. Rev. **116**, 7463–7500 (2016).
[106]P. H. Poole, F. Sciortino, U. Essmann, and H. E. Stanley, "Phase behaviour of metastable water," Nature **360**, 324–328 (1992).
[107]P. G. Debenedetti, F. Sciortino, and G. H. Zerze, "Second critical point in two realistic models of water," Science **369**, 289–292 (2020).
[108]K. Amann-Winkel, K. H. Kim, N. Giovambattista, M. Ladd-Parada, A. Späh, F. Perakis, H. Pathak, C. Yang, T. Eklund, T. J. Lane *et al.*, "Liquid-liquid phase separation in supercooled water from ultrafast heating of low-density amorphous ice," Nat. Commun. **14**(1), 442 (2023).
[109]K. H. Kim, K. Amann-Winkel, N. Giovambattista, A. Späh, F. Perakis, H. Pathak, M. L. Parada, C. Yang, D. Mariedahl, T. Eklund *et al.*, "Experimental observation of the liquid-liquid transition in bulk supercooled water under pressure," Science **370**(6519), 978–982 (2020).
[110]L. Perin and P. Gallo, "Phase diagram of aqueous solutions of LiCl: A study of concentration effects on the anomalies of water," J. Phys. Chem. B **127**(20), 4613–4622 (2023).
[111]J. Troncoso and D. González-Salgado, "The temperature of maximum density for aqueous solutions," J. Chem. Phys. **160**(10), 100902 ,(2024).
[112]S. Blazquez, M. de Lucas, C. Vega, J. Troncoso, and F. Gámez, "The temperature of maximum in density of aqueous solutions of nitrate and ammonium salts: Testing the Madrid-2019 force field," J. Chem. Phys. **161**, 046103 (2024).
[113]S. Blazquez and C. Vega, "Melting points of water models: Current situation," J. Chem. Phys. **156**(21), 216101 (2022).
[114]M. A. González and J. L. F. Abascal, "The shear viscosity of rigid water models," J. Chem. Phys. **132**, 096101 (2010).
[115]C. Q. Sun, C. Yao, Y. Sun, X. Liu, H. Fang, and Y. Huang, "(H, Li)Cl and LiOH hydration: Surface tension, solution conductivity and viscosity, and exothermic dynamics," J. Mol. Liq. **283**, 116–122 (2019).
[116]Y. Gao, J. Wu, Y. Feng, J. Han, and H. Fang, "Effects of hydrogen bond networks on viscosity in aqueous solutions," J. Phys. Chem. B **128**(37), 8984–8996 (2024).
[117]O. Butin, L. Pereyaslavets, G. Kamath, A. Illarionov, S. Sakipov, I. V. Kurnikov, E. Voronina, I. Ivahnenko, I. Leontyev, G. Nawrocki, M. Darkhovskiy, M. Olevanov, Y. K. Cherniavskyi, C. Lock, S. Greenslade, R. D. Kornberg, M. Levitt, and B. Fain, "The determination of free energy of hydration of water ions from first principles," J. Chem. Theory Comput. **20**(12), 5215–5224 (2024).
[118]C. Knight and G. A. Voth, "The curious case of the hydrated proton," Acc. Chem. Res. **45**, 101 (2012).
[119]P. Habibi, A. Rahbari, S. Blazquez, C. Vega, P. Dey, T. J. H. Vlugt, and O. A. Moultos, "A new force field for OH^- for computing thermodynamic and transport properties of H_2 and O_2 in aqueous NaOH and KOH solutions," J. Phys. Chem. B **126**(45), 9376–9387 (2022).
[120]P. Habibi, J. R. T. Postma, J. T. Padding, P. Dey, T. J. H. Vlugt, and O. A. Moultos, "Thermodynamic and transport properties of $H_2/H_2O/NaB(OH)_4$ mixtures using the Delft force field (DFF/$B(OH)_4^-$)," Ind. Eng. Chem. Res. **62**(30), 11992–12005 (2023).
[121]M. Laliberté and W. E. Cooper, "Model for calculating the density of aqueous electrolyte solutions," J. Chem. Eng. Data **49**(5), 1141–1151 (2004).
[122]L. Scalfi, L. Lehmann, A. P. Dos Santos, M. R. Becker, and R. R. Netz, "Propensity of hydroxide and hydronium ions for the air–water and graphene–water interfaces from *ab initio* and force field simulations," J. Chem. Phys. **161**(14), 144701 (2024).
[123]T. Lewis, B. Winter, A. C. Stern, M. D. Baer, C. J. Mundy, D. J. Tobias, and J. C. Hemminger, "Does nitric acid dissociate at the aqueous solution surface?," J. Phys. Chem. C **115**(43), 21183–21190 (2011).
[124]S. Baldelli, C. Schnitzer, and M. J. Shultz, "The structure of water on HCl solutions studied with sum frequency generation," Chem. Phys. Lett. **302**(1–2), 157–163 (1999).
[125]S. Blazquez, L. F. Sedano, and C. Vega, "On the compatibility of the Madrid-2019 force field for electrolytes with the TIP4P/ice water model," J. Chem. Phys. **161**, 224502 (2024).
[126]J. L. F. Abascal, E. Sanz, R. García Fernández, and C. Vega, "A potential model for the study of ices and amorphous water: TIP4P/ice," J. Chem. Phys. **122**, 234511 (2005).